iScience

CellPress
OPEN ACCESS

Article

Self-assembled peptides-modified flexible field-effect transistors for tyrosinase detection

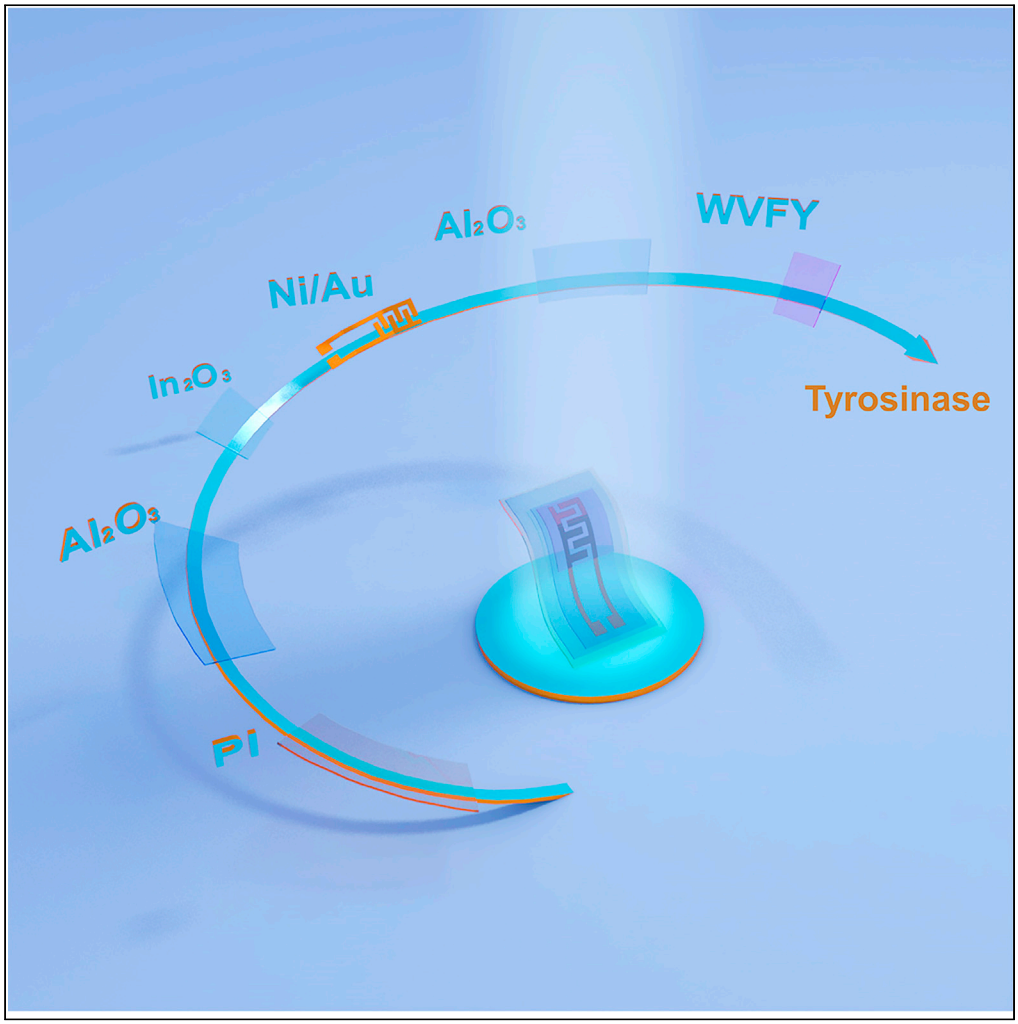

Huihui Ren, Tengyan Xu, Kun Liang, ..., Chunyan Song, Huaimin Wang, Bowen Zhu

wanghuaimin@westlake.edu.cn (H.W.)
zhubowen@westlake.edu.cn (B.Z.)

Highlights

Flexible and wearable biosensors based on peptides-modified metal oxide FETs

Biocompatible peptides form self-assembled nanostructures on flexible FETs

The biosensors convert tyrosinase concentration into changes in channel conductivity

The biosensors show an ultra-low detection limit for tyrosinase detection

Ren et al., iScience 25, 103673
January 21, 2022
https://doi.org/10.1016/j.isci.2021.103673

iScience

CellPress
OPEN ACCESS

Article

Self-assembled peptides-modified flexible field-effect transistors for tyrosinase detection

Huihui Ren,[1,2,6] Tengyan Xu,[3,6] Kun Liang,[1,2] Jiye Li,[1,2] Yu Fang,[3] Fanfan Li,[2,4] Yitong Chen,[1,2] Hongyue Zhang,[3] Dingwei Li,[1,2] Yingjie Tang,[1,2] Yan Wang,[1,2] Chunyan Song,[2] Huaimin Wang,[3,*] and Bowen Zhu[2,5,7,*]

SUMMARY

Flexible biosensors have received intensive attention for real-time, non-invasive monitoring of cancer biomarkers. Highly sensitive tyrosinase biosensors, which are important for melanoma screening, remained a hurdle. Herein, high-performance tyrosinase-sensing field-effect transistor-based biosensors (bio-FETs) have been successfully achieved by self-assembling nanostructured tetrapeptide tryptophan–valine–phenylalanine–tyrosine (WVFY) on n-type metal oxide transistors. In the presence of target tyrosinase, the phenolic hydroxyl groups in WVFY are rapidly converted to benzoquinone with the consumption of protons, which could be detected potentiometrically by bio-FETs. As a result, the WVFY-modified bio-FETs exhibited an ultra-low detection limit of 1.9 fM and an optimal detection range of 10 fM to 1 nM toward tyrosinase sensing. Furthermore, flexible devices fabricated on ~2.9-μm-thick polyimide (PI) substrates illustrated robust mechanical flexibility, which could be attached to human skin conformally. These achievements hold promise for wearable melanoma screening and provide designing guidelines for detecting other important cancer biomarkers with bio-FETs.

INTRODUCTION

As a type of malignant skin cancer along with high metastasis, recurrence, and mortality, melanoma has become a severe health-threatening problem worldwide (Huang et al., 2013; Sauer et al., 2017; Jang and Atkins, 2013). The incidence of cutaneous melanoma has risen rapidly over past several decades (Schadendorf et al., 2018; Leiter et al., 2020). Once tumors have spread to other organs, such skin cancer will quickly become lethal, owing to few treatment options and unsuccessful clinical trials (Schadendorf et al., 2018). Therefore, it is imperative to diagnose cancer in its early stages considering the rapid metastasis and evolution of melanoma.

To detect reliable melanoma biomarkers is one of the most effective strategies for the early diagnosis of cancer. Tyrosinase (TYR) has been proposed as a potential melanoma biomarker, because it overexpresses melanoma cells and accumulates in skin cells, closely related to the degree of malignancy (Welsh and Corrie, 2015; Robert et al., 2015). For example, high tyrosinase rate was observed in many patients with untreated melanoma at the late stage, while intervention treatment could decrease tyrosinase concentration, demonstrating that monitoring the dynamic change of tyrosinase concentration could provide a method of therapy prognosis to patients and a predictive factor for cancer evolution (Osella-Abate et al., 2003). The detection of tyrosinase is, therefore, crucial for practical clinical diagnosis and prognosis. Several laboratory-based methodologies have been developed for detecting tyrosinase activity, including fluorometry, colorimetry, spectrophotometry, electrochemistry (Zhan et al., 2018; Liu et al., 2013, 2017; Ciui et al., 2018; Fan et al., 2021).

Among them, field-effect transistor-based biosensor (bio-FET) has risen as a promising biosensing technology due to its point-of-care testing capabilities with high sensitivity and accuracy, intrinsic amplification, rapid and real-time feedback, and easy integration with complementary metal-oxide-semiconductor (CMOS) processors (Liu et al., 2017; Allen et al., 2007; Kim et al., 2020b). The specific interactions between

[1]Zhejiang University, Hangzhou 310027, China

[2]Key Laboratory of 3D Micro/Nano Fabrication and Characterization of Zhejiang Province, School of Engineering, Westlake University, Hangzhou 310024, China

[3]Key Laboratory of Precise Synthesis of Functional Molecules of Zhejiang Province, School of Science, Westlake University, Hangzhou 310024, China

[4]Key Laboratory of Wide Band Gap Semiconductor Technology, School of Microelectronics, Xidian University, Xi'an 710071, China

[5]Institute of Advanced Technology, Westlake Institute for Advanced Study, Hangzhou 310024, China

[6]These authors contributed equally

[7]Lead contact

*Correspondence: wanghuaimin@westlake.edu.cn (H.W.), zhubowen@westlake.edu.cn (B.Z.)

https://doi.org/10.1016/j.isci.2021.103673

target molecules and receptors modified on bio-FETs could alternate the potentials at the liquid/solid interface, resulting in variations in channel conductance. Also, the channel conductance can be modulated by conformational changes after receptors recognition or depended on alterations in surrounding environmental charges when exposure to target molecules (Bay et al., 2019). In addition, flexible and biocompatible bio-FETs could provide a new platform for continuously monitoring individuals' health in a wearable and continuous way, attracting widespread attention in recent years (Gao et al., 2016; Bariya et al., 2020; Tai et al., 2018; Li et al., 2020, 2021; Kim et al., 2020a). However, wearable bio-FETs capable of detecting early-stage melanoma remained a challenge (Emaminejad et al., 2017; Koh et al., 2016; Lee et al., 2016). Considering high mortality in the cancer stage and the colossal challenge of direct detection, it is significant to screen them in the early stage by monitoring biomarkers.

Here, we present a wearable tyrosinase-sensing bio-FET based on biocompatible self-assembled nanostructured peptides and n-type metal oxide FETs. The bio-FETs were achieved by solution-processed In_2O_3/Al_2O_3 semiconductor/dielectric interfaces, where In_2O_3 worked as the active channel and Al_2O_3 served as a passivation layer for preventing ion and water diffusion (Ren et al., 2021). By modifying a biocompatible tetrapeptide of tryptophan–valine–phenylalanine–tyrosine (WVFY) onto the In_2O_3/Al_2O_3 interfaces *via* self-assembly, the peptide-modified bio-FETs could successfully detect tyrosinase with high sensitivity, exhibiting an ultra-low detection limit of 1.9 fM and an optimal detection range of 10 fM to 1 nM. Furthermore, by fabricating Al_2O_3/In_2O_3 bio-FETs on ultrathin polyimide (PI) substrate (~2.9 μm thick), the devices could be attached to the skin conformally for wearable sensing applications. The results provide a flexible and biocompatible tyrosinase-sensing platform, promising for future melanoma screening applications.

RESULTS

The flexible Al_2O_3/In_2O_3-based bio-FETs with self-assembled nanostructured peptides were fabricated on ultrathin PI substrates (Figure S1). Figure 1A depicts the schematic illustration of the fabrication process (see Method details section). Typically, the ultrathin PI substrates were prepared *via* spin-coating PI solution on a carrier glass and subsequent annealing. Next, a thin layer of Al_2O_3 was spin-coated on PI film to serve as the barrier layer. Then, In_2O_3 precursor solution was spin-coated and annealed in air. Ni/Au electrodes were thermally evaporated to form source/drain (S/D) electrodes. The interdigitated S/D electrodes were utilized to generate strong electric fields and improve the active sensing region, which depicted low current crowding effects (Rim et al., 2015). Subsequently, another Al_2O_3 layer was spin-coated to serve as an effective barrier preventing ion and water diffusion to the underneath In_2O_3 channel. The as-fabricated bio-FETs were then mechanically delaminated from the carrier glass and could be transferred to other soft substrates, for example, polydimethylsiloxane (PDMS), to facilitate operation. Also, the ultrathin devices could be conformably attached to human skin at both flat and stretched states *via* van der Waals forces (Figure 1B).

Figures 1C and 1D depict the electrical performance of Al_2O_3/In_2O_3 bio-FETs before and after delamination from carrier glass and being transferred to a PDMS film, which was characterized in 0.1× phosphate-buffered saline (PBS) solution with a standard Ag/AgCl reference electrode as the gate electrode. Compared to the rigid substrates, the transfer characteristics (I_{ds}-V_{gs}, solid lines, Figure 1C) of the devices exhibited only tiny degradation when transferred to soft PDMS substrates. The corresponding threshold voltage (V_{th}) shift, current on/off ($I_{on/off}$) ratio, mobility (μ), and subthreshold swing (SS) change before and after transfer to PDMS are extracted in Table S1. Furthermore, the liquid-gated Al_2O_3/In_2O_3 bio-FETs demonstrated fast saturation behaviors and stable output currents with distinctive pinch-off characteristics, as shown in Figure 1D. The low operation voltage (<0.5 V) with small leakage current (I_{gs}, open circles, Figure 1C) benefits to avoid the redox reactions between the electrodes and biomolecules in the liquid environment, improving stability in long-term biomonitoring applications.

To characterize the mechanical flexibility and durability of flexible Al_2O_3/In_2O_3 bio-FETs, electrical bending tests under different bending radii and bending strain cycles were carried out. The device structure of an individual flexible bio-FET is shown in Figure 2A. Figure 2B shows a digital photo of the Al_2O_3/In_2O_3 bio-FET under the bending state, where a flexible polyethylene terephthalate (PET, ~50 μm thick) substrate was used to support the device to facilitate the bending test. The transfer curves of flexible Al_2O_3/In_2O_3 bio-FETs at the initial state and bending states with radii of ~2 and 1 cm are illustrated in Figure 2C, where almost no perceptible changes in electrical performance could be observed. To investigate mechanical

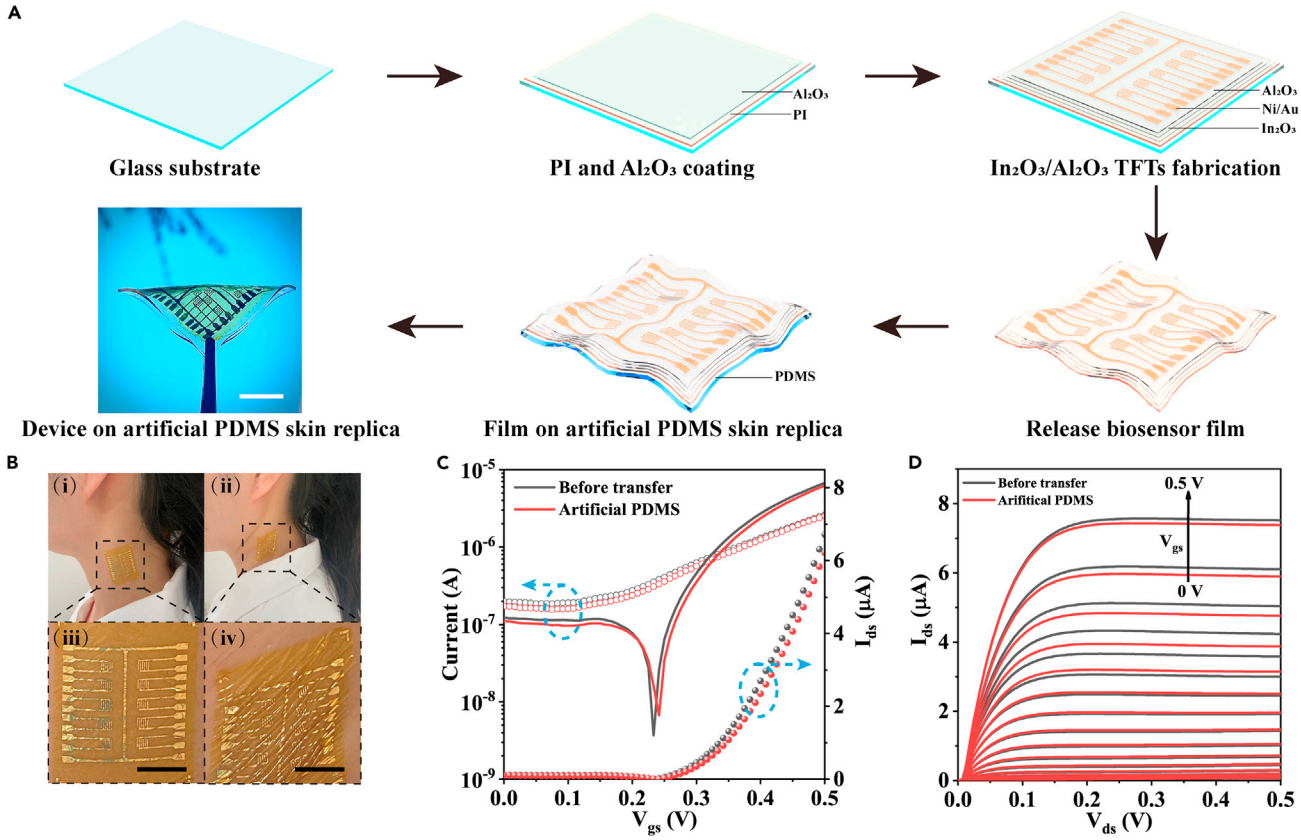

Figure 1. Process flow of flexible Al_2O_3/In_2O_3 FET-based conformal biosensors and their electrical characteristics

(A) Schematic showing the fabrication process of flexible bio-FETs. First, each glass substrate was coated with an ultrathin PI film, and a thin Al_2O_3 buffer layer was coated on the PI substrate. Next, In_2O_3 channel layer was spin-coated on PI film and baked at 300°C. Interdigitated source/drain electrodes of Ni/Au were patterned by shadow masks. Then Al_2O_3 precursor was spin coated on the UV-O_3 treated In_2O_3 devices to serve as the passivation layer. The PI films with Al_2O_3/In_2O_3 bio-FET arrays were then delaminated from the rigid glass substrate and transferred to PDMS. The thin PI films with Al_2O_3/In_2O_3 bio-FET arrays could conformally attached to PDMS.

(B) Digital photos of flexible Al_2O_3/In_2O_3 bio-FET arrays conformally attached to human neck skin in flat (i) and stretched (ii) states. (iii-iv) Magnified views of the black dashed regions in (i) and (ii), respectively. Scale bars: 50 μm.

(C) Transfer characteristics of Al_2O_3/In_2O_3 bio-FETs on rigid glasses and soft PDMS substrates measured in 0.1× PBS solution, illustrating similar electrical performance before and after being transferred to PDMS substrates. Solid lines: I_{ds} curves in logarithmic scales; solid circles: I_{ds} curves in linear scales; open circles: I_{gs} curves.

(D) Output curves of Al_2O_3/In_2O_3 bio-FETs on rigid glasses and flexible PDMS substrates, after transfer to soft PDMS substrates, the devices illustrated similar pinch-off characteristics under the Ag/AgCl liquid gating.

robustness, the devices were bent/released up to 1000 cycles with a bending radius of 1 cm, and no significant performance degradation was observed (Figure 2D). The corresponding V_{th} and SS values at different cycles are extracted in Figure 2E. Both SS and V_{th} showed minor variations from 70.9 ± 0.22 to 72.8 ± 1.4 mV dec^{-1} and from 0.38 ± 0.004 to 0.39 ± 0.005 V, respectively. Also, the corresponding variation of μ and $I_{on/off}$ ratio were illustrated in Figure S2, showing minor performance degradation from 0.66 ± 0.02 to 0.69 ± 0.02 $cm^2V^{-1}s^{-1}$ and from (6.5 ± 0.28) × 10^1 to (7.4 ± 0.33) × 10^1, respectively. Importantly, the devices exhibited high environmental stability. Figure 2F illustrates the electrical characteristics of flexible Al_2O_3/In_2O_3 bio-FETs measured at different times. The devices showed no obvious performance degradation up to 7 days. Hence, the robust mechanical flexibility and stable electrical performance render the Al_2O_3/In_2O_3 bio-FETs suitable for wearable and portable biosensing applications.

To enable the bio-FETs to detect tyrosinase, a significant biomarker for melanoma screening applications, we designed a tetrapeptide of WVFY with excellent self-assembly properties through π-π stacking (Adler-Abramovich et al., 2009; Wang et al., 2021) (Figure 3A). The WVFY was synthesized by standard Fmoc solid-phase peptide synthesis (SPPS) and purified by reverse-phase high-performance liquid chromatography

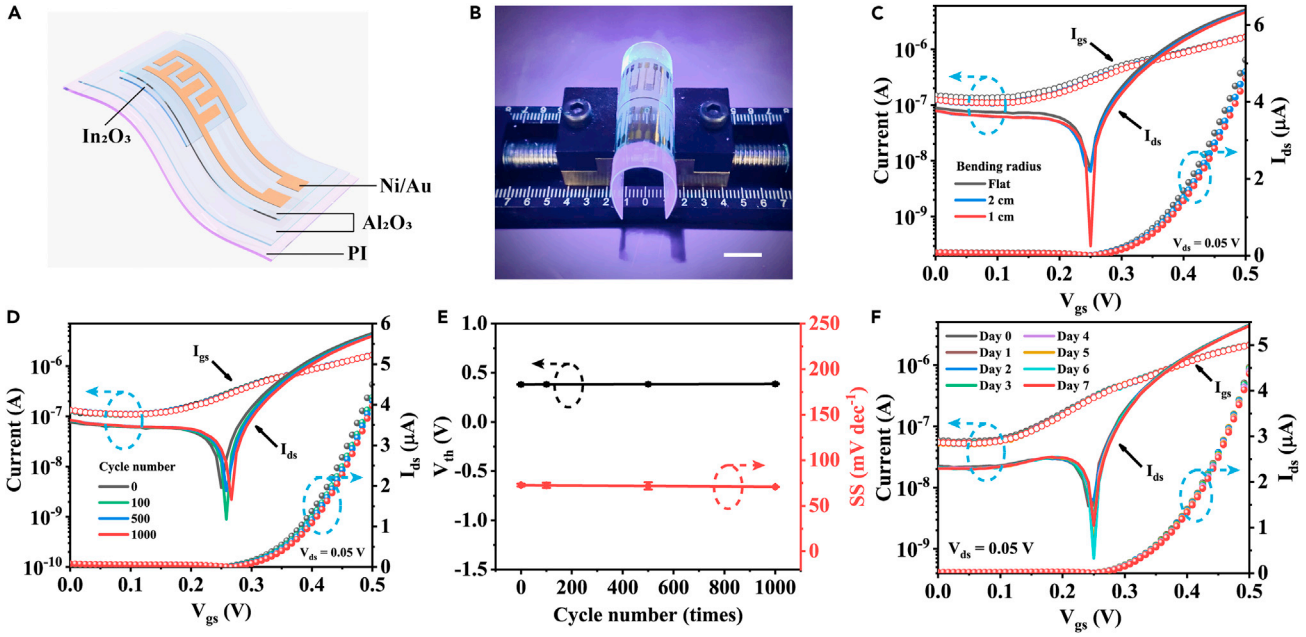

Figure 2. Electrical performance of flexible Al_2O_3/In_2O_3 bio-FETs

(A) Schematic illustration of the structure of a flexible Al_2O_3/In_2O_3 bio-FET

(B) A digital photo of the flexible device under bending. Scale bar: 1 cm.

(C) Transfer characteristics of the flexible Al_2O_3/In_2O_3 FETs at flat states (black) and under bending with bending radii of 2 (blue) and 1 cm (red). Solid lines: I_{ds} curves in logarithmic scales; solid circles: I_{ds} curves in linear scales; open circles: I_{gs} curves.

(D) Transfer characteristics of flexible Al_2O_3/In_2O_3 device after different bending test cycles with the bending radius of 1 cm. Solid lines: I_{ds} curves in logarithmic scales; solid circles: I_{ds} curves in linear scales; open circles: I_{gs} curves.

(E) Corresponding threshold voltage (V_{th}) and subthreshold swing (SS) values extracted from transfer curves as a function of bending test cycle number. Error bar stands for standard deviations of three tests.

(F) Transfer curves of the flexible device measured at different days. Solid lines: I_{ds} curves in logarithmic scales; solid circles: I_{ds} curves in linear scales; open circles: I_{gs} curves.

(HPLC) (Figures S3, S4, and S5). Typically, the WVFY film was prepared by dropping peptide solution in 1,1,1,3,3,3-hexafluoro-2-propanol (HFIP) on the bio-FET surface in air. When the peptide film was exposed to water vapor at 60°C for 12 h, the assembled nanostructures spontaneously grew on the film under the interaction of hydrogen bonds (peptide bonds and water molecules) and π-π stacking (between aromatic rings) (Figure S6). Figure 3B shows a top-view scanning electron microscopy (SEM) image of the assembled peptide film, indicating twisted fiber bundles. Next, we used circular dichroism spectra (CD) to characterize the structure of peptide film before and after water vapor treatment. As shown in Figure 1C, no obvious signal peak was found in the reference WVFY film, indicating no assembly occurred. In comparison, with water vapor treatment, the WVFY film showed a significant positive peak at around 202 nm and two negative peaks at around 222 and 235 nm, indicating the β-sheet-like arrangement (Figure 3C). Because the phenolic hydroxyl groups on WVFY could be oxidized by tyrosinase into melanin analogs, the WVFY film modified on bio-FETs could serve as the sensitive layer for tyrosinase detection (Lampel et al., 2017) (Figure S7).

Figures 4A and S8 illustrate the tyrosinase sensing setup and mechanism. The WVFY peptide film was self-assembled atop the Al_2O_3/In_2O_3 bio-FETs, forming a nanostructured film of ~6.6 μm thick (Figure S9). When the WVFY-modified bio-FETs were exposed to tyrosinase, the phenolic hydroxyl groups in WVFY would be oxidized to catechol and finally transferred to benzoquinone with the consumption of protons. The deprotonation of terminal groups on the bio-FETs would cause surface potential changes and result in channel conductance decrease due to electrostatic repulsion, which could be reflected by V_{th} shifts of bio-FETs. In this way, the concentration of tyrosinase could be quantified potentiometrically.

To verify the feasibility, we first quantified tyrosinase sensing performance of WVFY-modified Al_2O_3/In_2O_3 bio-FETs fabricated on rigid silicon substrates. As shown in Figure S10A, the transfer curves illustrate

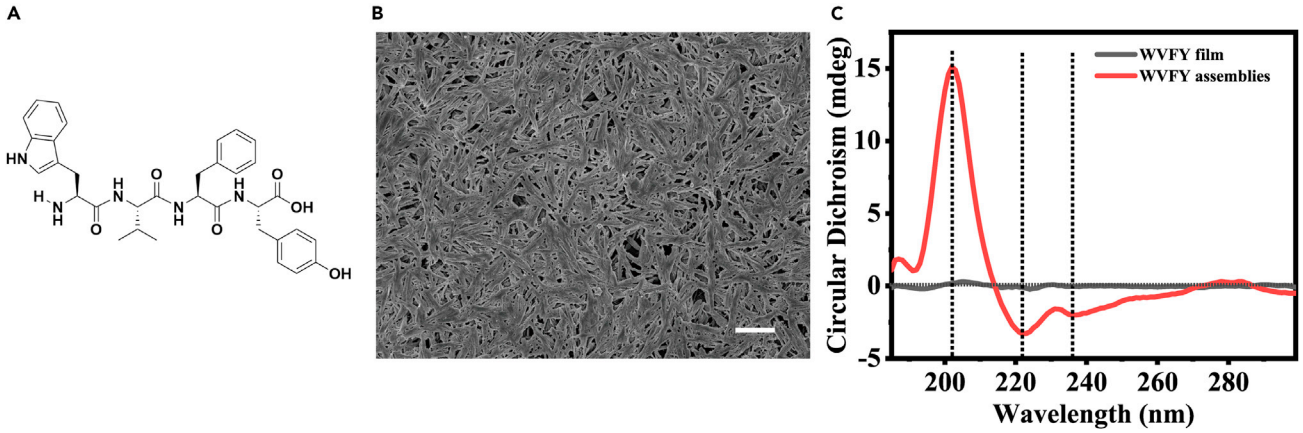

Figure 3. The characteristics of tetrapeptide tryptophan–valine–phenylalanine–tyrosine (WVFY) peptides

(A) The chemical structure of WVFY tetrapeptide.

(B) Top-view SEM image of the self-assembled WVFY nanostructured film by water vapor treatment at 60°C for 12 h. Scale bar: 10 μm.

(C) Circular dichroism spectra of WVFY films with (red) and without (black) assemblies.

characteristic positive shifts with an increase in the concentrations of tyrosinase (C_{TYR}) from 10 fM to 1 nM. As a result, the device showed a linear relationship (n = 3) between the ΔV_{th} and C_{TYR} on the logarithmic scale (Figure S10B). In comparison, the bio-FETs without self-assembled WVFY peptides were also investigated using the same sensing procedure, which showed no obvious V_{th} shifts but only with minor random variations (Figures S11A and S11B). Figure S12 illustrates the output characteristics of WVFY-modified bio-FETs when exposed to various C_{TYR}, where the saturation current decreases with the improvement of C_{TYR} corresponding to the depletion of protons. According to the equation of LOD (limit of detection) = 3.3 × SD of intercept/slop (Wang et al., 2017), where SD is the standard deviation of intercept, an outstanding LOD of 1.9 fM was extracted (Figures S13A and S13B). A comparison of the sensing performance of tyrosinase activity between our bio-FETs and documented methods (Ciui et al., 2018; Ding et al., 2021; Li et al., 2012, 2018; Liu et al., 2017; Wang et al., 2019; Yan et al., 2019; Yarman, 2018; Zhou et al., 2016) is shown in Table S2. Compared to previously reported methods for tyrosinase sensing, our bio-FETs are more advantageous in LOD with an acceptable linear range, which could be used as an accurate screening approach to monitor the tyrosinase level.

To explore the tyrosinase sensing performance of flexible devices, we further modified nanostructured WVFY peptides on bio-FETs fabricated on PI substrates with the same process. The typical transfer characteristics (I_{ds}-V_{gs}) of flexible devices at various C_{TYR} from 10 fM to 1 nM at a low drain bias (V_{ds}) of 0.05 V were plotted in Figure 4B. Still, the transfer curves shifted positively with the increase of C_{TYR}. In addition, the control devices whose surfaces were not functionalized with WVFY peptides were also studied with the same procedure for comparison. In the absence of WVFY peptides, tyrosinase itself was not puissant enough to influence electrostatic interaction on the surface of bio-FETs. Therefore, only minute and random fluctuations in the family of transfer curves were observed (Figure 4C). The linear relationships between ΔV_{th} and C_{TYR} of the flexible bio-FETs with/without WVFY peptides are depicted in Figure 4D. Furthermore, the flexible WVFY-modified bio-FETs exhibited stable and fast saturation with distinctive pinch-off behaviors as shown in Figure 4E. Also, the saturation current decreased gradually with the improvement of C_{TYR} from 10 fM to 1 nM. The result was consistent with the transfer characteristics (Figure 4B), owing to the depletion of electrons and decreased channel conductivity.

Reproducibility is one of the most significant parameters of sensor response, which is strongly related to sensor reliability and consistency (Najafi et al., 2019). It could be indexed by the coefficient of vibration (CV) using the following equations (Chen et al., 2020):

$$Coefficient\ of\ variation\ (CV) = \frac{Standard\ deviation}{Average\ of\ detection\ value} \times 100\% \quad \text{(Equation 1)}$$

$$Reproducibility = 100\% - CV \quad \text{(Equation 2)}$$

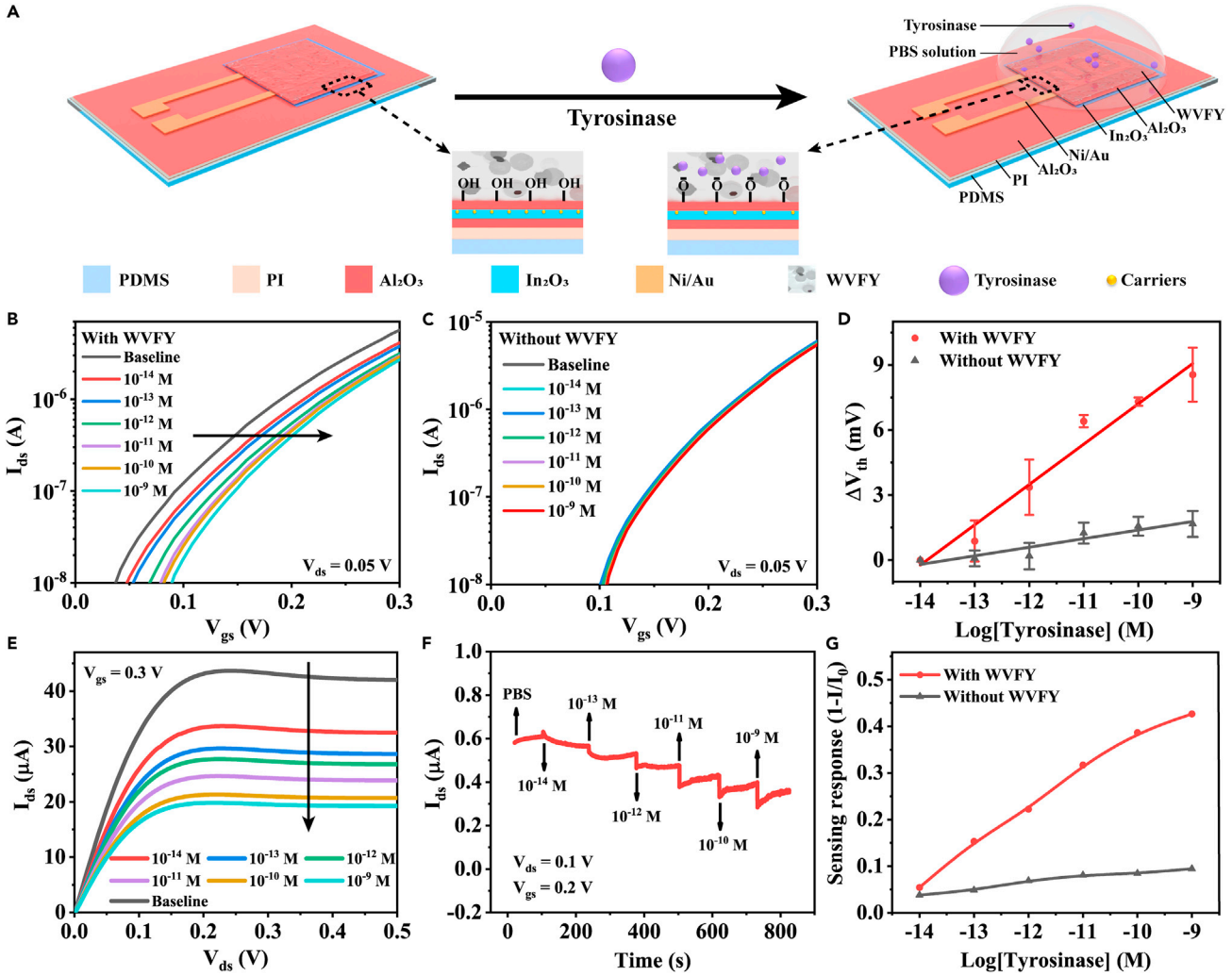

Figure 4. Tyrosinase-sensing performance of nanostructured WVFY peptides-modified flexible Al_2O_3/In_2O_3 bio-FETs

(A) Schematic illustration of the flexible Al_2O_3/In_2O_3 bio-FETs functionalized with WVFY peptides in response to tyrosinase and sensing mechanism. In the presence of tyrosinase, the phenolic hydroxyl group in WVFY will be oxidized to catechol and finally transferred to benzoquinone with the consumption of protons. This could be detected potentiometrically by measuring the channel conductivity.

(B) Family of typical transfer curves of WVFY-modified bio-FETs measured in 0.1× PBS solution with various concentrations of tyrosinase: baseline (black), 10^{-14} M (red), 10^{-13} M (deep blue), 10^{-12} M (green), 10^{-11} M (purple), 10^{-10} M (ginger), and 10^{-9} M (sky blue). The V_{th} shifted positively with increased tyrosinase concentration (C_{TYR}).

(C) A family of transfer curves of Al_2O_3/In_2O_3 bio-FETs without WVFY peptides when exposed to different C_{TYR}, illustrating minor response.

(D) Linear relationships between the ΔV_{th} and C_{TYR} in logarithmic scale. Error bars indicate the standard deviations of three repeated tests with $p < 0.05$.

(E) Output characteristics of flexible WVFY-modified bio-FETs configured by varying C_{TYR}. The I_{ds} decreased with the improvement of C_{TYR}, which was in line with the transfer performance. The applied gate bias was 0.3 V.

(F) Real-time sensing response of flexible WVFY-modified bio-FETs with tyrosinase. The drain and gate voltage (V_{ds} and V_{gs}) were 0.1 and 0.2 V, respectively.

(G) Relationships between the sensing response ($1 - I/I_0$) and C_{TYR}.

The average reproducibility of about 82% was obtained with the WVFY-modified bio-FET for monitoring various concentrations of tyrosinase (Figure S14).

In addition, we also carried out additional experiments to evaluate the durability. The sensitivity of the WVFY-modified bio-FET was tested after the device was stored in air for one week. As shown in Figure S15, the bio-FET showed the same detection range of 10 fM to 1 nM, when compared to the original device (Figures 4B and 4D), which demonstrated high durability and environmental stability.

To further investigate the electrical performance of flexible devices, real-time sensing response was characterized. As shown in Figure 4F, the drain current (I_{ds}) decreases with the accumulation of tyrosinase from 10 fM to 1 nM. The I_{ds}-*time* curve was also measured for referenced bio-FETs without WVFY, showing no obvious response (Figure S16). The relationship of the sensing response (1 - I/I_0) as a function of C_{TYR} of flexible devices with/without WVFY was illustrated in Figure 4G. The WVFY-modified bio-FETs exhibited a much higher response than the control devices, illustrating the importance of WVFY in tyrosinase detection. In contrast, the increased sensing response in control devices may originate from the current drift.

It was reported that the sensitivity is closed related to the transconductance when the V_{gs} was fixed (Kang et al., 2021; Rim, 2020; Chen et al., 2017). Figure S17A shows the I_{ds} and g_m increased with the improvement of V_{gs}, where the maximum g_m of 70.0 μS was achieved at V_{gs} = 0.3 V and V_{ds} = 0.05 V. Subsequently, time-resolved response (*time*-I/I_0) of the bio-FETs with or without WVFY modification was characterized in PBS at V_{gs} = 0.3 V and V_{ds} = 0.05 V. As depicted in Figure S17B, an increased I/I_0 response of WVFY-modified bio-FETs was obtained upon 10 fM to 1 nM tyrosinase. In comparison, the bare devices (without WVFY) only exhibited a small current vibration without obvious response (Figure S17C). Figure S17D shows the relationship between the sensing response (1 - I/I_0) and the tyrosinase concentration on the logarithm scale. It is noted that the devices with WVFY have a maximum sensing response of 0.82 approximately, much higher than the control group (0.09), when the V_{ds} and V_{gs} were fixed at 0.05 and 0.3 V, respectively.

As shown in Figure S18 (Figure S18 is the time extension of Figure S17B), after the addition of 1 × 10^{-9} M tyrosinase, certain amount of PBS solution was injected (at ~660 s) to dilute the tyrosinase concentration from 1 × 10^{-9} to 1 × 10^{-10} M again. The normalized current (I/I_0) did not return to the previous value with 1 × 10^{-10} M. On the contrary, after dilution from 1 × 10^{-9} to 1 × 10^{-10} M with PBS, the sensing response didn't change much (saturated), owing to the non-reversible reaction between the phenolic hydroxyl groups and catechol in WVFY.

We further demonstrate the application of WVFY peptide-modified bio-FET for living cells detection. Two different kinds of cell lines, B16F10 and HeLa cells were chosen to regard melanoma cells with overexpressed tyrosinase and non-melanoma cancer cells with low tyrosinase expression, respectively (Suzuki et al., 1994; White and Hu, 1977). Therefore, B16F10 and HeLa cells were selected as the model cell line and the negative control group, respectively. As shown in Figures S19A and S19B, the normalized current (I/I_0) decreases with the density of B16F10 cells accumulated from 0.5 × 10^4 to 2 × 10^5 cells mL^{-1}, owing to the increase of tyrosinase concentration. The real-time sensing response was also measured in HeLa cell lysates, demonstrating no significant sensing signals. The sensing response (1 - I/I_0) as a function of cell densities was depicted in Figure S19C, illustrating the feasibility of the bio-FETs in distinguishing these two kinds of cells.

DISCUSSION

We have described flexible tyrosinase-sensing bio-FETs based on biocompatible self-assembled WVFY peptide nanostructures. The devices exhibited outstanding mechanical flexibility and could be conformally attached to the skin for future wearable sensing applications. The sensing response of the devices originated from the specific reactions between tyrosinase and phenolic hydroxyl groups in WVFY, which consume protons and cause the surface potential change on the bio-FET. As a result, the channel conductivity decreased, and V_{th} shifted positively with elevated tyrosinase concentration. Notably, the devices showed an ultralow detection limit of 1.9 fM with a detection range of 10 fM to 1 nM by virtue of the intrinsic amplification of bio-FETs. Taking full advantages of high sensitivity, excellent mechanical flexibility, and low-cost solution-based processibility, the self-assembled peptide-modified bio-FETs offer considerable promise for tyrosinase detection and melanoma screening. In addition, the flexible and biocompatible bio-FETs open new opportunities for future health monitoring in a wearable manner. Still, our strategy of applying peptide-modified bio-FETs could be extended to the detection of other important cancer biomarkers by the exquisite design of functional peptides and FETs, promising for obviating invasive biopsy and delays in related diseases.

Limitations of the study

Our method provides a FET-based sensor platform capable of detecting tyrosinase levels. However, large-scale quantitative investigations aimed at tyrosinase detection at different stages of cancer are required to utilize the bio-FETs for the future real-world practice of melanoma detection, as tyrosinase shows different

activity levels when patients are at different cancer stages. In addition, the accuracy of this approach after extensive melanoma screening needed to be further verified.

STAR★METHODS

Detailed methods are provided in the online version of this paper and include the following:

- KEY RESOURCES TABLE
- RESOURCE AVAILABILITY
  - Lead contact
  - Materials availability
  - Data and code availability
- METHOD DETAILS
  - Materials
  - Preparation of precursor solution
  - Flexible Al_2O_3/In_2O_3 devices fabrication
  - Peptide synthesis
  - Formation of WVFY assemblies
  - Tyrosinase detection in cell lysate
  - Characterization
- QUANTIFICATION AND STATISTICAL ANALYSIS

SUPPLEMENTAL INFORMATION

Supplemental information can be found online at https://doi.org/10.1016/j.isci.2021.103673.

ACKNOWLEDGMENTS

We acknowledge financial support from the National Natural Science Foundation of China (Grant No. 62174138), and the Westlake Multidisciplinary Research Initiative Center (MRIC) (Grant No. MRIC20200101). We thank Westlake Center for Micro/Nano Fabrication, and the Instrumentation and Service Center for Physical Sciences (ISCPS), and the Instrumentation and Service Center for Molecular Sciences (ISCMS) at Westlake University for the facility support and technical assistance.

AUTHOR CONTRIBUTIONS

Data were collected by H.R., T.X., and K.L., and analyzed by H.R., T.X., F.L., H.Z., D.L., Y.T., Y.W., H.W., and B.Z. Figures were prepared by H.R., T.X., J.L., Y.C., and C.S. The manuscript was written by H.R., T.X., H.W, and B.Z. with assistance from all authors. All authors have given approval to the final version of the manuscript.

DECLARATION OF INTERESTS

The authors declare no competing interests.

Received: October 6, 2021
Revised: November 30, 2021
Accepted: December 16, 2021
Published: January 21, 2022

REFERENCES

Adler-Abramovich, L., Aronov, D., Beker, P., Yevnin, M., Stempler, S., Buzhansky, L., Rosenman, G., and Gazit, E. (2009). Self-assembled arrays of peptide nanotubes by vapour deposition. Nat. Nanotechnol. *4*, 849–854. https://doi.org/10.1038/nnano.2009.298.

Allen, B.L., Kichambare, P.D., and Star, A. (2007). Carbon nanotube field-effect-transistor-based biosensors. Adv. Mater. *19*, 1439–1451. https://doi.org/10.1002/adma.200602043.

Bariya, M., Li, L., Ghattamaneni, R., Ahn, C.H., Nyein, H.Y.Y., Tai, L.-C., and Javey, A. (2020). Glove-based sensors for multimodal monitoring of natural sweat. Sci. Adv. *6*. eabb8308. https://doi.org/10.1126/sciadv.abb8308.

Bay, H.H., Vo, R., Dai, X., Hsu, H.H., Mo, Z., Cao, S., Li, W., Omenetto, F.G., and Jiang, X. (2019). Hydrogel gate graphene field-effect transistors as multiplexed biosensors. Nano Lett. *19*, 2620–2626. https://doi.org/10.1021/acs.nanolett.9b00431.

Chen, H., Rim, Y.S., Wang, I.C., Li, C., Zhu, B., Sun, M., Goorsky, M.S., He, X., and Yang, Y. (2017). Quasi-two-dimensional metal oxide semiconductors based ultrasensitive potentiometric biosensors. ACS Nano. *11*, 4710–4718. https://doi.org/10.1021/acsnano.7b00628.

Chen, L.-C., Wang, E., Tai, C.-S., Chiu, Y.-C., Li, C.-W., Lin, Y.-R., Lee, T.-H., Huang, C.-W., Chen, J.-C., and Chen, W.L. (2020). Improving the reproducibility, accuracy, and stability of an electrochemical biosensor platform for point-of-

care use. Biosens. Bioelectron. *155*, 112111. https://doi.org/10.1016/j.bios.2020.112111.

Ciui, B., Martin, A., Mishra, R.K., Brunetti, B., Nakagawa, T., Dawkins, T.J., Lyu, M., Cristea, C., Sandulescu, R., and Wang, J. (2018). Wearable wireless tyrosinase bandage and microneedle sensors: toward melanoma screening. Adv. Healthc. Mater. *7*. e1701264. https://doi.org/10.1002/adhm.201701264.

Ding, X.M., Cai, S.X., Wang, L., and Zhang, Y.C. (2021). Electrocatalytic performance of tyrosinase detection in Penaeus vannamei based on a [(PSS/PPy)(P2Mo18/PPy)5] multilayer composite film modified electrode. Anal. Methods *13*, 1392–1403. https://doi.org/10.1039/d0ay02328k.

Emaminejad, S., Gao, W., Wu, E., Davies, Z.A., Nyein, H.Y.Y., Challa, S., Ryan, S.P., Fahad, H.M., Chen, K., and Shahpar, Z. (2017). Autonomous sweat extraction and analysis applied to cystic fibrosis and glucose monitoring using a fully integrated wearable platform. Proc. Natl. Acad. Sci. U S A *114*, 4625–4630. https://doi.org/10.1073/pnas.1701740114.

Fan, Y.-F., Zhu, S.-X., Hou, F.-B., Zhao, D.-F., Pan, Q.-S., Xiang, Y.-W., Qian, X.-K., Ge, G.-B., and Wang, P. (2021). Spectrophotometric assays for sensing tyrosinase activity and their applications. Biosensors *11*, 290. https://doi.org/10.3390/bios11080290.

Gao, W., Emaminejad, S., Nyein, H.Y.Y., Challa, S., Chen, K., Peck, A., Fahad, H.M., Ota, H., Shiraki, H., Kiriya, D., et al. (2016). Fully integrated wearable sensor arrays for multiplexed in situ perspiration analysis. Nature *529*, 509–514. https://doi.org/10.1038/nature16521.

Huang, F.W., Hodis, E., Xu, M.J., Kryukov, G.V., Chin, L., and Garraway, L.A. (2013). Highly recurrent TERT promoter mutations in human melanoma. Science *339*, 957–959. https://doi.org/10.1126/science.1229259.

Jang, S., and Atkins, M.B. (2013). Which drug, and when, for patients with BRAF-mutant melanoma? Lancet Oncol. *14*, e60–e69. https://doi.org/10.1016/S1470-2045(12)70539-9.

Kang, H., Wang, X., Guo, M., Dai, C., Chen, R., Yang, L., Wu, Y., Ying, T., Zhu, Z., Wei, D., et al. (2021). Ultrasensitive detection of SARS-CoV-2 antibody by graphene field-effect transistors. Nano Lett. https://doi.org/10.1021/acs.nanolett.1c00837.

Kim, H., Kim, Y.S., Mahmood, M., Kwon, S., Epps, F., Rim, Y.S., and Yeo, W.H. (2020a). Wireless, continuous monitoring of daily stress and management practice via soft bioelectronics. Biosens. Bioelectron. *173*, 112764. https://doi.org/10.1016/j.bios.2020.112764.

Kim, H., Rim, Y.S., and Kwon, J.-Y. (2020b). Evaluation of metal oxide thin-film electrolyte-gated field effect transistors for glucose monitoring in small volume of body analytes. IEEE Sens. J. *20*, 9004–9010. https://doi.org/10.1109/jsen.2020.2988269.

Kim, M.G., Kanatzidis, M.G., Facchetti, A., and Marks, T.J. (2011). Low-temperature fabrication of high-performance metal oxide thin-film electronics via combustion processing. Nat. Mater. *10*, 382–388. https://doi.org/10.1038/nmat3011.

Koh, A., Kang, D., Xue, Y., Lee, S., Pielak, R.M., Kim, J., Hwang, T., Min, S., Banks, A., Bastien, P., et al. (2016). A soft, wearable microfluidic device for the capture, storage, and colorimetric sensing of sweat. Sci. Transl. Med. *8*. 366ra165. https://doi.org/10.1126/scitranslmed.aaf2593.

Lampel, A., Mcphee, S.A., Park, H.-A., Scott, G.G., Humagain, S., Hekstra, D.R., Yoo, B., Frederix, P.W., Li, T.-D., and Abzalimov, R.R. (2017). Polymeric peptide pigments with sequence-encoded properties. Science *356*, 1064–1068. https://doi.org/10.1126/science.aal5005.

Lee, H., Choi, T.K., Lee, Y.B., Cho, H.R., Ghaffari, R., Wang, L., Choi, H.J., Chung, T.D., Lu, N.S., Hyeon, T., et al. (2016). A graphene-based electrochemical device with thermoresponsive microneedles for diabetes monitoring and therapy. Nat. Nanotechnol. *11*, 566–572. https://doi.org/10.1038/nnano.2016.38.

Leiter, U., Keim, U., and Garbe, C. (2020). Epidemiology of Skin Cancer: Update 2019. *Sunlight, Vitamin D and Skin Cancer* (Springer)), pp. 123–139.

Li, D., Du, J., Tang, Y., Liang, K., Wang, Y., Ren, H., Wang, R., Meng, L., Zhu, B., and Li, Y. (2021). Flexible and air-stable near-infrared sensors based on solution-processed inorganic–organic hybrid phototransistors. Adv. Funct. Mater. https://doi.org/10.1002/adfm.202105887.

Li, D., Zhao, M., Liang, K., Ren, H., Wu, Q., Wang, H., and Zhu, B. (2020). Flexible low-power source-gated transistors with solution-processed metal-oxide semiconductors. Nanoscale *12*, 21610–21616. https://doi.org/10.1039/d0nr06177h.

Li, H., Liu, W., Zhang, F., Zhu, X., Huang, L., and Zhang, H. (2018). Highly selective fluorescent probe based on hydroxylation of phenylboronic acid pinacol ester for detection of tyrosinase in cells. Anal. Chem. *90*, 855–858. https://doi.org/10.1021/acs.analchem.7b03681.

Li, S., Mao, L., Tian, Y., Wang, J., and Zhou, N. (2012). Spectrophotometric detection of tyrosinase activity based on boronic acid-functionalized gold nanoparticles. Analyst *137*, 823–825. https://doi.org/10.1039/c2an16085d.

Liu, B.-W., Huang, P.-C., Li, J.-F., and Wu, F.-Y. (2017). Colorimetric detection of tyrosinase during the synthesis of kojic acid/silver nanoparticles under illumination. Sens. Actuators, B *251*, 836–841. https://doi.org/10.1016/j.snb.2017.05.129.

Liu, X., Wang, F., Niazov-Elkan, A., Guo, W., and Willner, I. (2013). Probing biocatalytic transformations with luminescent DNA/silver nanoclusters. Nano Lett. *13*, 309–314. https://doi.org/10.1021/nl304283c.

Najafi, V., Zolghadr, S., and Kimiagar, S. (2019). Remarkable reproducibility and significant sensitivity of ZnO nanoparticles covered by chromium (III) oxide as a hydrogen sulfide gas sensor. Optik *182*, 249–256. https://doi.org/10.1016/j.ijleo.2019.01.015.

Osella-Abate, S., Savoia, P., Quaglino, P., Fierro, M.T., Leporati, C., Ortoncelli, M., and Bernengo, M.G. (2003). Tyrosinase expression in the peripheral blood of stage III melanoma patients is associated with a poor prognosis: a clinical follow-up study of 110 patients. Br. J. Cancer *89*, 1457–1462. https://doi.org/10.1038/sj.bjc.6601197.

Park, S., Lee, S., Kim, C.H., Lee, I., Lee, W.J., Kim, S., Lee, B.G., Jang, J.H., and Yoon, M.H. (2015). Sub-0.5 V highly stable aqueous salt gated metal oxide electronics. Sci. Rep. *5*, 13088. https://doi.org/10.1038/srep13088.

Ren, H., Liang, K., Li, D., Zhao, M., Li, F., Wang, H., Miao, X., Zhou, T., Wen, L., Lu, Q., et al. (2021). Interface engineering of metal-oxide field-effect transistors for low-drift pH sensing. Adv. Mater. Inter. https://doi.org/10.1002/admi.202100314.

Rim, Y.S. (2020). Review of metal oxide semiconductors-based thin-film transistors for point-of-care sensor applications. J. Inf. Disp. *21*, 203–210. https://doi.org/10.1080/15980316.2020.1714762.

Rim, Y.S., Bae, S.-H., Chen, H., Yang, J.L., Kim, J., Andrews, A.M., Weiss, P.S., Yang, Y., and Tseng, H.-R. (2015). Printable ultrathin metal oxide semiconductor-based conformal biosensors. ACS Nano. *9*, 12174–12181. https://doi.org/10.1021/acsnano.5b05325.

Robert, C., Schachter, J., Long, G.V., Arance, A., Grob, J.J., Mortier, L., Daud, A., Carlino, M.S., Mcneil, C., and Lotem, M. (2015). Pembrolizumab versus ipilimumab in advanced melanoma. N. Engl. J. Med. *372*, 2521–2532. https://doi.org/10.1056/NEJMoa1503093.

Sauer, A.G., Siegel, R.L., Jemal, A., and Fedewa, S.A. (2017). Updated review of prevalence of major risk factors and use of screening tests for cancer in the United States. Cancer Epidemiol. Biomarkers Prev. *26*, 1192–1208. https://doi.org/10.1158/1055-9965.EPI-17-0219.

Schadendorf, D., Van Akkooi, A.C., Berking, C., Griewank, K.G., Gutzmer, R., Hauschild, A., Stang, A., Roesch, A., and Ugurel, S. (2018). Melanoma. Lancet *392*, 971–984. https://doi.org/10.1016/S0140-6736(18)31559-9.

Suzuki, H., Takahashi, K., Yasumoto, K.-I., and Shibahara, S. (1994). Activation of the tyrosinase gene promoter by neurofibromin. Biochem. Biophys. Res. Commun. *205*, 1984–1991. https://doi.org/10.1006/bbrc.1994.2903.

Tai, L.C., Gao, W., Chao, M., Bariya, M., Ngo, Q.P., Shahpar, Z., Nyein, H.Y.Y., Park, H., Sun, J., Jung, Y., et al. (2018). Methylxanthine drug monitoring with wearable sweat sensors. Adv. Mater. *30*. e1707442. https://doi.org/10.1002/adma.201707442.

Wang, H., Yao, S., Liu, Y., Wei, S., Su, J., and Hu, G. (2017). Molecularly imprinted electrochemical sensor based on Au nanoparticles in carboxylated multi-walled carbon nanotubes for sensitive determination of olaquindox in food and feedstuffs. Biosens. Bioelectron. *87*, 417–421. https://doi.org/10.1016/j.bios.2016.08.092.

Wang, J., Li, Q., Hu, L., Wang, Y., Qi, W., Su, R., and He, Z. (2021). Self-assembly of ferrocenyl phenylalanine into nanohelical arrays via kinetic control. ACS Appl. Bio Mater. *4*, 4744–4752. https://doi.org/10.1021/acsabm.0c00607.

Wang, L., Gan, Z.F., Guo, D., Xia, H.L., Patrice, F.T., Hafez, M.E., and Li, D.W. (2019). Electrochemistry-regulated recyclable SERS sensor for sensitive and selective detection of tyrosinase activity. Anal. Chem. *91*, 6507–6513. https://doi.org/10.1021/acs.analchem.8b05341.

Welsh, S.J., and Corrie, P.G. (2015). Management of BRAF and MEK inhibitor toxicities in patients with metastatic melanoma. Ther. Adv. Med. Oncol. *7*, 122–136. https://doi.org/10.1177/1758834014566428.

White, R., and Hu, F. (1977). Characteristics of tyrosinase in B16 melanoma. J. Invest. Dermatol. *68*, 272–276. https://doi.org/10.1111/1523-1747.ep12494214.

Yan, K., Ji, W., Zhu, Y., Chen, F., and Zhang, J. (2019). Photofuel cell coupling with redox cycling as a highly sensitive and selective self-powered sensing platform for the detection of tyrosinase activity. Chem. Commun. *55*, 12040–12043. https://doi.org/10.1039/c9cc05649a.

Yarman, A. (2018). Development of a molecularly imprinted polymer-based electrochemical sensor for tyrosinase. Turk. J. Chem. *42*, 346–354. https://doi.org/10.3906/kim-1708-68.

Zhan, C., Cheng, J., Li, B., Huang, S., Zeng, F., and Wu, S. (2018). A fluorescent probe for early detection of melanoma and its metastasis by specifically imaging tyrosinase activity in a mouse model. Anal. Chem. *90*, 8807–8815. https://doi.org/10.1021/acs.analchem.8b00594.

Zhou, J., Shi, W., Li, L., Gong, Q., Wu, X., Li, X., and Ma, H. (2016). Detection of misdistribution of tyrosinase from melanosomes to lysosomes and its upregulation under psoralen/ultraviolet A with a melanosome-targeting tyrosinase fluorescent probe. Anal. Chem. *88*, 4557–4564. https://doi.org/10.1021/acs.analchem.6b00742.

STAR★METHODS

KEY RESOURCES TABLE

REAGENT or RESOURCE	SOURCE	IDENTIFIER
Biological samples		
Tyrosinase	MERCK	T3824-25KU; CAS:9002-10-2
Chemicals, peptides, and recombinant proteins		
Indium (III) nitrate hydrate (99.999%)	Sigma-Aldrich	CAS: 207398-97-8
Aluminum (III) nitrate nonahydrate (99.997%)	Sigma-Aldrich	CAS: 7784-27-2
Poly(pyromellitic dianhydride-co-4,4′-oxydianiline), amic acid solution (12 wt.%)	Sigma-Aldrich	SKU: 575771
Polydimethylsiloxane (Sylgard 184) curing agent and base	Dow Corning Corporation	Sylgard 184
Fmoc-Trp (Boc)-OH	GL Biochem	CAS:143824-78-6
Fmoc-Val-OH	GL Biochem	CAS:68858-20-8
Fmoc-Phe-OH	GL Biochem	CAS:35661-40-6
Fmoc-Tyr(tBu)-OH	GL Biochem	CAS:71989-38-3
Hexafluoroisopropanol		MERYER CO., LTD
Experimental models: Cell lines		
HeLa cells	Cellcook Biotech Co.,Ltd.	CC1101
B16F10 cells	Cellcook Biotech Co.,Ltd.	CC9016
Software and algorithms		
Origin	Headquartered in Northampton, Massachusetts, USA	www.originlab.com
Keysight EasyEXPERT	Keysight Technologies	www.keysight.com

RESOURCE AVAILABILITY

Lead contact

Further information and requests for resources and reagents should be directed to and will be fulfilled by the lead contact, Dr. Bowen Zhu (zhubowen@westlake.edu.cn).

Materials availability

All materials generated in this study are available from the lead contact without restriction.

Data and code availability

Data reported in this paper will be shared by the lead contact upon request. This study did not generate/analyze code. Any additional information required to reanalyze the data reported in this paper is available from the lead contact upon request.

METHOD DETAILS

Materials

Indium (III) nitrate hydrate ($In(NO_3)_3 \cdot xH_2O$, 99.999%), aluminum (III) nitrate nonahydrate ($Al(NO_3)_3 \cdot 9H_2O$, 99.997%) and poly(pyromellitic dianhydride-co-4,4′-oxydianiline), amic acid solution (PI, 12 wt.%) were purchased from Sigma-Aldrich. 2-methoxyethanol (2-ME, 99.3%, Alfa Aesar), acetylacetone (AcAc, 99%, Alfa Aesar), and ammonium hydroxide ($NH_3 \cdot H_2O$, 28%, Alfa Aesar) were used as received. Fmoc-amino acids were obtained from GL Biochem (Shanghai). 2-Cl-trityl chloride resin was obtained from Nankai Resin Co. Ltd. (Tianjin). Polydimethylsiloxane (PDMS, Sylgard 184) curing agent and base were obtained from Dow Corning Corporation. Silicon wafer with 100 nm thick SiO_2 layer was obtained from Silicon Valley

Microelectronics, Inc. Commercially available reagents were used without further purification unless noted otherwise.

Preparation of precursor solution

The In_2O_3 (0.1 M) and Al_2O_3 (0.1 M) precursor solutions were prepared *via* dissolving 0.30 g $In(NO_3)_3 \cdot xH_2O$ and 0.38 g $Al(NO_3)_3 \cdot 9H_2O$ in 10 mL 2-ME mixed with 100 μL AcAc and 35 μL $NH_3 \cdot H_2O$, respectively. AcAc and $NH_3 \cdot H_2O$ were used as additives to improve electrical performance, owing to the combustion reaction (Kim et al., 2011). The prepared precursor solutions were stirred vigorously at room temperature for 24 h, then filtered via a 0.2 μm organic syringe filter prior to use.

Flexible Al_2O_3/In_2O_3 devices fabrication

Ultrathin (~2.9 μm thick) polyimide (PI) substrates were prepared by spin coating PI solution on cleaned glasses at 1000 rpm/min for 60 s, and then baked at elevated temperatures of 150, 200, and 250°C, each for 30 min, and finally annealed at 300°C for 1 hour at a nitrogen-filled glove box. 0.2 M Al_2O_3 precursor solution was spin-coated on ultraviolet-ozone (UV-O_3) treated PI films and then annealed at 300°C for 1 h to form thin buffer layers. A thin In_2O_3 channel layer was deposited on UV-O_3 treated PI substrates by spin-coating 0.1 M In_2O_3 precursor solution at 3000 rpm/min for 30 s, followed by annealing at 300°C for 1 h in air. After that, the source and drain electrodes of Ni/Au (8/30 nm) were deposited by thermal evaporation with shadow masks, forming a channel width/length (W/L) of 7500 μm/200 μm, respectively. To prepare Al_2O_3/In_2O_3 devices, 0.1 M Al_2O_3 precursor was spin-coated on the UV-O_3 treated In_2O_3 devices to serve as the passivation layer and annealed at 300°C for 1 h, protecting the semiconductor layer from ion diffusion and water diffusion.

Peptide synthesis

WVFY was synthesized by solid phase peptide synthesis (SPPS) using 2-chlorotrityl chloride resin, and the side chains of the corresponding N-Fmoc protected amino acids are appropriately protected by different groups. Firstly, the C-terminal of the first amino acid was conjugated on the resin. Anhydrous *N,N'*-dimethyl formamide (DMF) containing 20% piperidine was used to remove Fmoc protected group. To couple the next amino acid to the free amino group, O-(Benzotriazol-1-yl)-*N,N,N',N'*-tetramethyluronium hexafluorophosphate (HBTU) was used as coupling reagent. The growth of the peptide chain was according to the established Fmoc SPPS protocol. After the last coupling step, the sample was washed with DMF for 1 minute (5 mL per gram of resin) for 3 times to remove excess reagents, then washed with DCM for 1 minute (5 mL per gram of resin) for another 3 times. The peptide was cleaved using 95% of trifluoroacetic acid (TFA) with 2.5% of triisopropylsilane (TIS) and 2.5% of H_2O for 60 minutes. 20 mL per gram of resin of ice-cold diethyl ether was then added to the concentrated cleavage reagent. The resulting precipitate was centrifuged for 10 min at 4°C at 5000 rpm. Afterward the supernatant was decanted, and the resulting solid was dissolved in H_2O/CH_3CN (1:1) for HPLC separation using CH_3CN and H_2O containing 0.1% of TFA as eluents.

Formation of WVFY assemblies

WVFY was first dissolved in hexafluoroisopropanol (HFIP) at a concentration of 160 mM at 25°C. After vortex for 1.5 min, the mixtures were allowed to stand for 30 minutes. Then, 20 μL of the solutions were dropped on the surface of FETs. The samples were placed in a vacuum desiccator and vacuumed for 2 minutes to form the peptide film. Finally, the FET was stuck on the top of a chromatographic bottle, then put the bottle in a screw-cap vial involving 3 ml H_2O. Then, the vial was put into an oven installed with designed temperature (60°C) during the growth of the assemblies.

Tyrosinase detection in cell lysate

Cells (B16F10 and HeLa) were seeded in cell culture dish with MEM (Minimum Essential Medium)/RPMI (Roswell Park Memorial Institute) 1640 culture medium containing 10% fetal bovine serum and 1% penicillin-streptomycin. After incubation for 24 h, the upper solution was removed and then washed three times with PBS buffer. The remaining cells were ultrasonically cleaved in PBS buffer at 0°C, then the lysates were collected and centrifuged at 14,000 rpm for 15 min at 4°C. The supernatants were collected to detect tyrosinase activities inside of cells.

Characterization

The synthesized compounds were characterized using ^1H NMR (Bruker AVANCE NEO 500 MHz). HPLC was conducted at Agilent 1260 Infinity II Manual Preparative Liquid Chromatography system using a C18 RP

column with CH_3CN (0.1% of TFA) and water (0.1% of TFA) as the eluents. LC-MS was conducted at the Agilent Infinity Lab LC/MSD system. Circular dichroism (CD) spectra were measured by an Applied Photophysics Ltd (Chirascan V100) system. All the samples were placed into quartz spectrophotometer cell and the wavelength range was from 185 to 300 nm and the step was 1 nm. The resultant CD spectrum was acquired after subtracting the solvent background. The samples for SEM analysis were coated with platinum on a High Vacuum Coating instrument (Leica, EM ACE600), and then characterized by a Regulus 8230 field emission SEM (Hitachi High-tech Corp., Japan) at the acceleration voltage of 3.0 kV. The thickness of PI film was obtained by a surface profile measuring system (Bruker, Dektak XT). Electrical characteristics were performed in dry and liquid environments by a semiconductor parameter analyzer (4200A-SCS, Keithley) and/or source meter (Agilent B2912A). The mobility (μ) and subthreshold swing (SS) were extracted from the transfer curves using the equation of

$$\mu = \frac{L}{WC_{EDL}V_{ds}}\left(\frac{\partial I_{ds}}{\partial V_{gs}}\right) \quad \text{(Equation 3)}$$

, and

$$SS = \frac{\partial V_{gs}}{\partial(\log_{10} I_{ds})} \quad \text{(Equation 4)}$$

, where C_{EDL} is the electrical double layer capacitance in 0.1 M ionic strength solution (25.52 $\mu F \cdot cm^{-2}$) (Park et al., 2015). V_{ds}, V_{gs}, and I_{ds} stand for drain voltage, gate voltage, and drain current, respectively. W and L are channel width and length of the transistors.

QUANTIFICATION AND STATISTICAL ANALYSIS

Origin software were used to compile and analyze data. Error bars stood for means $\pm$ SD. $p < 0.05$ was considered to be statistically significant. The details of statistical methods could be found in Figure Legends and results.